THE JOURNAL OF PHYSICAL CHEMISTRY B

Article

pubs.acs.org/JPCB

Solvation and Rotation Dynamics in the Trihexyl(tetradecyl)phosphonium Chloride Ionic Liquid/Methanol Cosolvent System

Kathleen M. Barra, Randy P. Sabatini,† Zachery P. McAtee, and Mark P. Heitz*

Department of Chemistry, The College at Brockport, State University of New York, Brockport, New York 14420, United States

Supporting Information

ABSTRACT: The interactions and solvent structure in trihexyl(tetradecyl)phosphonium chloride ionic liquid ($[P_{14,6,6,6}^+][Cl^-]$, "PIL-Cl")/methanol (MeOH) solutions across the entire range of mole fraction PIL-Cl (x_{IL} = 0−1) are discussed. Viscosity and conductivity measurements are used to characterize the bulk solvent properties. At x_{IL} < 0.1, the log(η) data show a nonlinear dependence on mole fraction in contrast to the data for x_{IL} > 0.1 where the data vary linearly with mole fraction. Conductivity data show a maximum at x_{IL} = 0.03 in good agreement with conductivity measurements in imidazolium ILs. Steady-state and time-resolved fluorescence spectroscopies were used to measure the equilibrium, lifetime, and rotational response of coumarin 153 (C153) in neat and MeOH cosolvent modified PIL-Cl. The collective set of data depicts the formation of an increasingly aggregated solvent structure that changes in proportion to the amount of PIL-Cl present in MeOH. Average solvation and rotation times are found to scale with solution viscosity. At x_{IL} values of 0.02−0.2, the rotation times are at or near the hydrodynamic stick limit, whereas for x_{IL} > 0.2 rotation times drop to between 40 and 70% of the stick limit, consistent with the IL literature. In this cosolvent system, the most dramatic changes in solution behavior occur between 0 and 10% PIL-Cl.

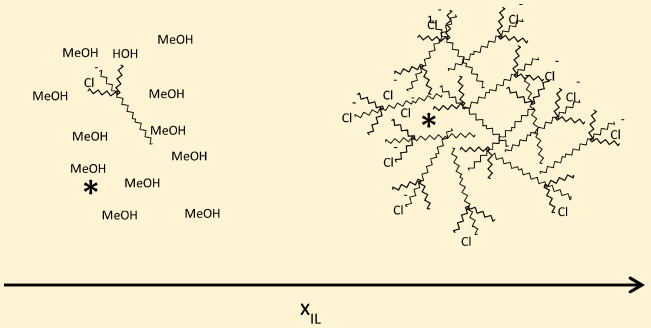

I. INTRODUCTION

Room temperature ionic liquids have become a popular medium for synthetic chemistry and a broad range of chemical applications.[1−5] Ionic liquids (ILs) are commonly considered to be "environmentally friendly" solvents, and thus, there is considerable interest in using ILs to serve as alternatives to traditional organic solvents. Moreover, there are large numbers of cation/anion combinations that can be used to create designer solvents or task-specific ILs.

Over the past decade, a large body of experimental[6−15] and computational[16−24] work has focused on characterizing physicochemical properties,[6,12−14,17,25] investigating the solubility of small molecules,[8,14] and describing cosolvent interactions using a wide variety of organic solvents.[11,12,26−40] Interactions between ILs and dense gas/supercritical fluids (e.g., CO_2) have also been studied.[8,41−45] Equilibrium solvation in ILs is commonly probed by measuring the steady-state absorption and fluorescence emission of a dye molecule in order to elucidate the dependence of a probe's spectral shift on changes in solvent reorganization, whereas time-resolved (fluorescence) emission spectra (TRES) are measured to provide insight on the dynamics of molecular solvation. In addition, anisotropy measurements yield an additional perspective on solvation dynamics via characterization of the microscopic friction a solute experiences as solute and solvent reorganization take place. Solvation dynamics have been described using computer simulations,[18,19,23,24] Stokes shift measurements,[10,35−38,40,46−55] and rotational dynamics[9,32,35−38,40,46−49,51−55] measurements. Recently, a semi-molecular theory has been developed to investigate the Stokes shift dynamics in both neat ILs and binary solvent/IL mixtures and to provide a quantitative comparison between theory and measurements.[56−59] In neat ILs, ion−dipole (IL−solute) forces are dominant[23,51,55] but solvent−solvent, including ion−ion[60] and dispersion forces, and dipolar forces[55] can also be expected to contribute strongly to solvation. In solvent/IL mixtures, solvent reorganization dynamics are inherently complex because of the multiplicity of interactions that take place between the solute, cosolvent, and the IL cation−anion pair. Conventional dipolar solvents couple strongly to dipolar solutes primarily through dipole−dipole forces, and this is the major contribution to solvation and relaxation processes. The presence of a molecular cosolvent further complicates the complete set of interactions by introducing additional forces that depend strongly on the specific cosolvent/IL pair used, which has been presented quantitatively from a theoretical perspective.[57,59] In both neat ILs and IL/solvent mixtures, one expects the solvation dynamics to be responsive to the varying

Received: September 13, 2014
Revised: October 15, 2014
Published: October 16, 2014

types of molecular interactions; however, this is not always the case.[37,40,51−53] For example, Samanta and co-workers report that when nonpolar solvents were added to the ion pair 1-butyl-3-methylimidazolium hexafluorophosphate ($[bmim]^+[PF_6]^-$) the rotational dynamics of coumarin 153 (C153) becomes faster due to a lowering of overall solvent viscosity.[40] A similar observation was reported by Sarkar and co-workers studying C153 and 1-hexyl-3-methylimidazolium hexafluorophosphate ($[hmim]^+[PF_6]^-$) where the addition of polar solvents, both protic and aprotic solvent types, also caused faster rotational dynamics because of lower viscosity.[37] Whether the solvent was nonpolar, protic, or aprotic, the primary effect is credited to solvent viscosity as opposed to specific solute/cosolvent/IL interactions. However, they did note that the rotational dynamics of C153 in the binary mixtures of IL + polar solvents was less pronounced compared to the binary mixtures of IL + aprotic solvent.[37] Maroncelli and co-workers also reported that the C153 average solvation times vary essentially linearly with viscosity in neat ILs spanning several classes that included imidazolium, ammonium, and phosphonium cations.[52,53] In this measure, IL solutions are a linear extension of conventional dipolar solvents. The role that cosolvent interactions play in modified IL systems is still a topic of significant interest.[10,11,19,27−40,61−71]

A vast amount of the IL literature has focused on the C_2-C_6 imidazolium cations paired with a wide variety of anions. The phosphonium class of ILs has received much less attention, though they offer a wide range of attractive physical properties[72,73] and electrochemical properties.[74] In this work, we focus on the solvation of C153 in trihexyl(tetradecyl)-phosphonium chloride ionic liquid ($[P_{14,6,6,6}^+][Cl^-]$, "PIL-Cl"; Scheme 1), both neat and modified with methanol (MeOH).

Scheme 1. Structures of the Probe Coumarin 153 (C153)

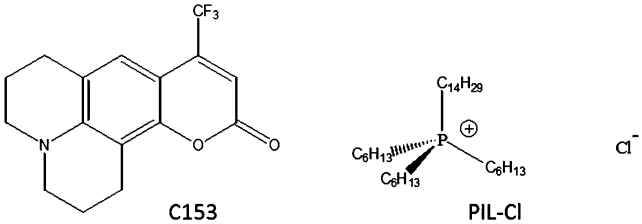

We report briefly on the bulk solution physical properties, which include viscosity and conductivity measurements, and on the steady-state and time-resolved fluorescence emission to support the discussion of solvation in this IL system. All optical measurements were made using the solvatochromic probe coumarin 153 (C153; Scheme 1). Intensity decay (lifetime) measurements were made using the time-correlated single photon counting (TCSPC) method. The extensive body of IL literature that describes solvation, including both computational (simulations) and experimental techniques, is used to discuss the results of our work.

II. MATERIALS AND EXPERIMENTAL METHODS

Coumarin 153 (laser grade) was purchased from Exciton, stored under desiccation, and used as received. The phosphonium IL was synthesized by Cytec Canada Inc.[75] and dried in a vacuum oven for 5 days at 45 °C prior to use. MeOH was HPLC grade from Fisher Scientific. Two methods were used to prepare the cosolvent solutions for spectroscopic analysis. To prepare a MeOH-rich solution, a stock 1 mM C153/MeOH was added to the cuvette and diluted to 2 mL such that [C153] = 10 μM (optical density was always less than 0.1). PIL-Cl solutions were made by massing PIL-Cl directly into the cuvette. The cuvette was always kept tightly stoppered to minimize MeOH evaporative loss. To equilibrate these solutions, the cuvette was repeatedly inverted until a single-phased solution was achieved. All spectroscopic measurements were made on the same solution, after which more PIL-Cl was added to the same cuvette. In this way, successive additions to the same cuvette were made up to x_{IL} = 0.12. To make PIL-Cl-rich solutions, a known mass of PIL-Cl was first warmed until it was fluid enough to easily stir. Then, an appropriate amount of C153/MeOH stock solution was gently added to the PIL-Cl surface so that the MeOH evaporated prior to mixing. As before, [C153] was 10 μM. The solution was stirred for a minimum of 10 min to achieve homogeneity and then was poured into a pre-massed cuvette and then re-massed. All spectroscopic measurements were made on this solution prior to micropipetting additions of MeOH to make the next mole fraction solution. In this way, mole fraction was varied down to x_{IL} = 0.068. Independent of the preparation method, solutions were always single-phased and optically transparent at all mole fraction compositions studied. The uncertainty in mole fraction was less than ±0.5%.

The water content of each solution component was determined by Karl Fischer coulometric titration using a Mettler Toledo C20 titrator equipped with a DM 143-SC double platinum pin electrode at 295 K. Measurements were performed in triplicate, and average values are reported. The water content of MeOH was 130 ± 2 ppm. Since the neat PIL-Cl is highly viscous, direct injection into the apparatus was impossible. Therefore, approximately 1 g of IL was dissolved in 2 mL of MeOH and this solution was used to determine the IL water content. Replicate measurements showed that the PIL-Cl contained 0.12 ± 0.06 wt % water so reference to "neat" PIL-Cl or x_{IL} = 1 must be kept in this context. While this amount of water is larger than typically reported (usually <100 ppm), water content above 1000 ppm was used in previous work with PILs but its presence was undetectable in the measurements.[47,50,52,76]

"Neat" and cosolvent modified PIL-Cl densities and viscosities were measured using an Anton-Paar DM4100 density meter coupled with an AMVn automated rolling ball viscometer. Rolling angles were accurate to 0.1°, and temperature was controlled to ±0.02 K. Capillary sizes used were 1.6, 1.8, 3.0, and 4.0 mm depending on the amount of PIL-Cl in solution, and they were calibrated using a Koehler Instrument Company, Inc., ISO 17025 Viscosity and Density Reference Standard, type S60 or type S600. In a typical viscosity measurement, temperature was varied from 278 to 323 K and four to six rolling angles were measured at each temperature. Data were collected in a cyclical fashion by starting at low temperature and increasing to the maximum and then cooling down to the original value. In this way, we were able to check reproducibility and check for any hysteresis effects. For all measurements, uncertainty was typically ±1−2% and reproducibility was ±0.5−1%.

Bulk solution conductivity measurements were made using a Fisher Scientific Accumet AB30 conductivity meter equipped with a two-cell platinized electrode (model number 13-620-157). Conductivity was measured at room temperature, 295.0 ± 0.1 K. The cell constant was determined prior to

measurements using certified NIST SRM 3193 traceable KCl conductivity standard solutions, 1413 ± 1 and 10000 ± 10 μS/cm at 25 °C from Ricca Chemical Company.

Steady-state absorption was measured using a PerkinElmer Lambda 800 UV−vis spectrometer operating at 1 nm resolution. Fluorescence excitation and emission data were collected using a Horiba Scientific (Spex) Fluorolog-3 fluorescence spectrometer with 2 nm resolution. Briefly, a 450 W Xe arc lamp was used to excite the samples through a single grating monochromator and the emission wavelength was selected using a double grating monochromator to enhance stray light rejection and detected using a Hamamatsu R928P PMT. The signal-to-noise ratio was always at least 5000:1. The instrument was calibrated using the water Raman signal at the start of each day, and all spectra were blank subtracted and corrected for instrument response.

Time-resolved emission intensity decays were measured using the Fluorolog 3 instrument, modified with time-correlated single photon counting (TCSPC) components from Horiba Scientific. The excitation source was a 405 nm NanoLED (405-L) high output diode laser operating at a 1 MHz repetition rate, controlled through a FluoroHub-NL software plug-in accessory card designed for use with the FluoroHub controller module run by DataStation software. Excitation photons were passed through a vertically aligned polarizer before entering the sample, housed in a Starna Cells, Inc., 23-Q-10 Spectrosil 1 cm stoppered quartz cuvette. The sample emission was passed through a Glan-Thompson polarizer set at "magic" angle (54.7°) and spectrally resolved using the Fluorolog-3 double grating monochromator prior to detection with a cooled photocathode IBH TBX 850 detector. The instrument response was measured using a scattering solution, and typical values for the instrument response of this system were routinely on the order of 170−190 ps per pulse. Emission intensity decay was measured over a 50 ns time window (~8000 channels) using a bin size of 6.8 ps per channel. All decay data were measured at the peak of the steady-state emission with emission slits no greater than 8 nm. Taken together, the instrument response function and the intensity decay data were fit to a sum of exponentials models using an iterative reconvolution algorithm contained within the IBH DAS6 decay analysis software. After reconvolution, the estimated effective time resolution was ~40 ps. The quality of fit to a specific model was assessed using reduced chi-squared values (χ_r^2), and a fit was judged to be acceptable if $\chi_r^2 < 1.2$. When the data seemed to require a multiexponential decay model, we allowed the inclusion of an additional time constant only if there was at least a 10% improvement (decrease) in χ_r^2 along with a discernible improvement in fit residuals and/or the fitted autocorrelation function.

III. EXPERIMENTAL RESULTS

A. Bulk Properties—Density, Viscosity, and Conductivity. Density, viscosity, and conductivity were measured from x_{IL} = 0 to 1. Density data are reported in Table S1 (Supporting Information). Viscosity and conductivity data are summarized in Figures 1 and 2, respectively. Both sets of data are typical of what is observed in IL/cosolvent solutions. For $x_{IL} < 0.1$, the change in viscosity is relatively small and varies by about an order of magnitude from neat MeOH to x_{IL} = 0.1; see Figure 1. We also note that in this range Δ log(η) shows a nonlinear dependence on log(x_{IL}). For $x_{IL} > 0.1$, log(η) varies nearly linearly with respect to log(x_{IL}) (r^2 = 0.947) and the viscosity

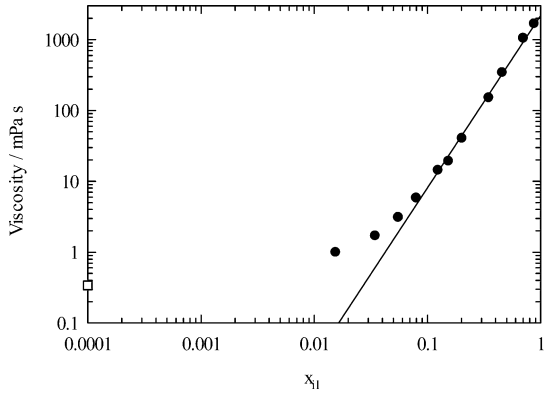

Figure 1. Viscosity of PIL-Cl at 295 K. The open square (□) located on the *y*-axis is data in neat MeOH, x_{IL} = 0.

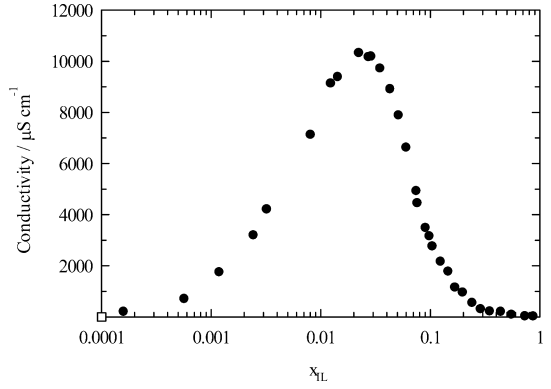

Figure 2. Conductivity of PIL-Cl at 295 K. The open square (□) located on the *y*-axis is data in neat MeOH, x_{IL} = 0.

changes by 3 orders of magnitude between x_{IL} = 0.1 and 1. We also examined log(η) plotted against PIL-Cl molar concentration (Figure S1, Supporting Information) and note that those data are nonlinear at all but the last three IL additions (r^2 = 0.997). Plotted in this way, the linear response threshold occurs at x_{IL} ~0.5 or 50 mol % PIL-Cl.

The conductivity data in Figure 2 show a maximum at x_{IL} = 0.025, where there is a 10 000-fold increase in solution conductance relative to the MeOH background (2 μS/cm, shown as an open square, □) and neat IL (13 μS/cm, x_{IL} = 1). Using dielectric spectroscopic measurements, Buchner and coworkers reported the observation of a similar peak in the data at low x_{IL} in an imidazolium IL, though the magnitude of the change is not as large.[69] Other reports also show the same behavior.[77,78] In dilute IL solution, there are relatively few charge carriers, but as PIL-Cl is added, the conductivity increases rapidly to a maximum. Although further addition of PIL-Cl increases the number of charge carriers the conductivity rapidly drops off because the increasing solvent viscosity limits ion mobility. Figure S2 (Supporting Information) shows the conductivity data plotted against PIL-Cl molar concentration. In this construct, the conductivity shows a linear behavior up to a solution concentration of about 0.1 M PIL-Cl.

B. Steady-State Spectroscopy. Steady-state absorption and emission spectra of neat PIL-Cl and C153/PIL-Cl solutions were measured as a function of x_{IL} in MeOH. Although neat PIL-Cl showed an intrinsic fluorescence emission (λ_{ex} = 405 nm), it was on the order of only a few percent of the intensity observed in C153/PIL-Cl; see Figure

dx.doi.org/10.1021/jp5092784 | J. Phys. Chem. B 2014, 118, 12979−12992

S3 (Supporting Information). Representative steady-state emission spectra are shown in Figure 3 and are typical of

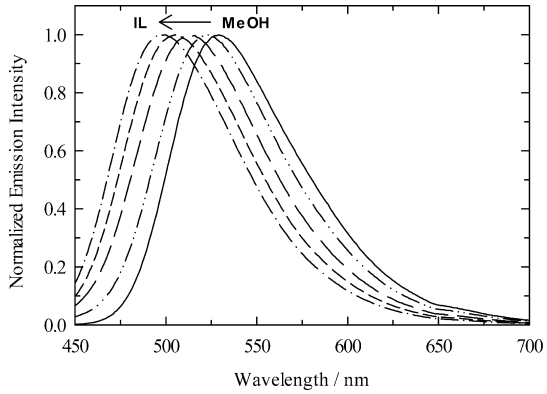

Figure 3. Representative normalized steady-state emission spectra for C153 in PIL-Cl/MeOH at 295 K. From left to right, mole fractions of PIL-Cl shown are x_{IL} = 1.00, 0.517, 0.349, 0.133, and 0.00.

spectra observed in simple polar solvents. C153 spectra in various ILs are all similar and independent of specific cation/anion pairs.[37,47,54,79] The spectra are broad and featureless, and the emission spectral shapes are the typical fluorescence log-normal line shape. Figure 4 summarizes the relative steady-state intensities, peak frequencies, and full width at half-maximum (fwhm). A general observation is that the data in any one parameter clearly show at least two distinct trends. The PIL-Cl spectra show a systematic hypsochromic shift of ~25 nm on increasing PIL-Cl across the entire range of mole fraction (x_{IL} = 0 → 1). In neat MeOH, the C153 emission maximum occurs at ~530 nm (=18 870 cm^{-1}), whereas the peak emission in neat PIL-Cl is ~504 nm (=19 840 cm^{-1}).

Spectral intensity in Figure 4 shows that very small additions of PIL-Cl to MeOH (x_{IL} < 0.001) result in measurable changes. For example, at x_{IL} = 0.001, we observe a 10% drop in fluorescence intensity. The intensity decrease continues to a minimum value at x_{IL} = 0.025, at which the relative intensity has dropped by about 55%. In contrast, at low x_{IL}, the peak position and fwhm are relatively insensitive and remain essentially constant until x_{IL} ~0.1. While the changes in position and width are readily understood in the context of C153's local environment, the intensity data require further comment. One interpretation of intensity variation is that changes in the probe's microenvironment cause a change in relaxation pathways, which alters the radiative rate constant (k_{rad}). If a change in microenvironment is accompanied by the enhancement of nonradiative pathways (k_{nr}), this will be manifested as an intensity decrease. Moreover, the presence of increased numbers of ions can also influence k_{rad}, as has been demonstrated by the increase of nonradiative rates in electrolyte solutions of ethyl acetate.[80] Another possibility for intensity change is simply concentration change. In these experiments, solutions were produced by the subsequent addition of either PIL-Cl or MeOH to the prior solution, which results in both dilution and increased electrolyte concentration. Therefore, an intensity decrease is not surprising. We used measured densities (reported in Table S1, Supporting Information) and calculated the solution excess volume on addition of PIL-Cl to MeOH; for x_{IL} = 0–0.025, the percent volume increase is about 35%, and for x_{IL} = 0–0.1, it is about 170% increase. Qualitatively, the trend up to x_{IL} = 0.025

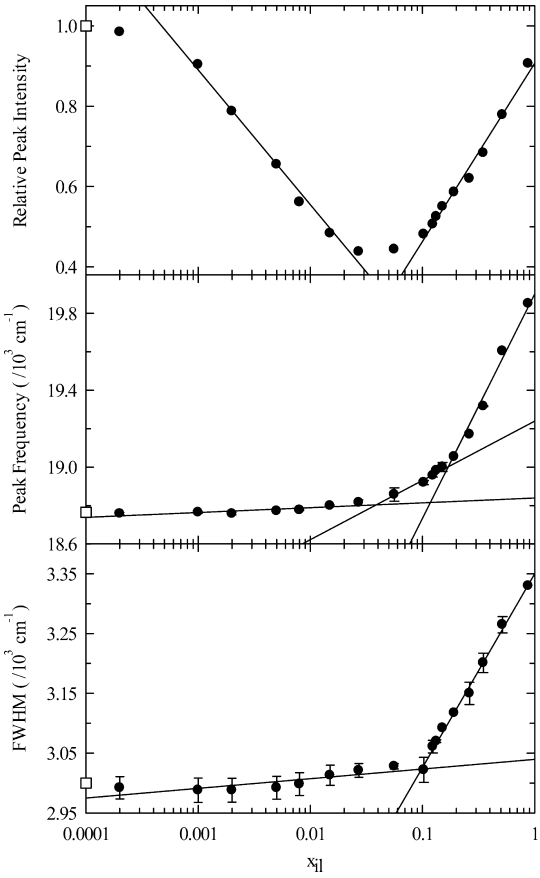

Figure 4. Steady-state spectral parameters for C153/PIL-Cl/MeOH. Lines are simple linear regression fits to a subset of data at or near the apparent breaks in the data and are intended to help visualize the trends. The relative intensity in the top panel was calculated by using the intensity of C153 in neat MeOH as the reference intensity. The open squares (□) located on each of the *y*-axes are data in neat MeOH, x_{IL} = 0.

scales with the measured intensity change but dilution alone does not account for the entire intensity change for two reasons. First, the magnitude of the intensity decrease at x_{IL} = 0.025 is 55% and the total volume change is only 35%. Second, the intensity *increases* from x_{IL} = 0.025 to 0.10.

It is interesting to note the point at which solution composition causes a significant change in each of the steady-state parameters. To approximate the x_{IL} value at each apparent break, a subset of data on each side of the assumed transition in each plot was chosen such that the variation in the selected points was linear. Using these points, we computed simple linear regressions and the intersection of each set of lines was the estimated x_{IL} transition point. The absolute values of the slopes in the intensity plot are within 10% of one another, supporting the idea that dilution effects are similar for sample preparation from each composition extreme. Emission maximum and fwhm data show slopes increase by a factor of ~20 at x_{IL} ~0.1. From the regressions, we estimate that the intensity minimum is at x_{IL} = 0.06 and the peak position and fwhm have minima at x_{IL} = 0.11 and 0.10, respectively. We interpret these steady-state results as clear indications that significant organizational change occurs at a solution composition of 10% PIL-Cl.

C. Time-Resolved Spectroscopy. Magic angle intensity decays of C153 in PIL-Cl/MeOH at 295 K were measured at

dx.doi.org/10.1021/jp5092784 | J. Phys. Chem. B 2014, 118, 12979–12992

the emission maximum of each solution mole fraction, across the range of x_{IL} studied. The fact that there was detectable fluorescence emission from the PIL-Cl blank necessitated that we attempt to measure its lifetime under conditions identical to the C153 experiments, including the length of time for a typical intensity decay acquisition (~5 min). However, the amount of signal was <10 cps and therefore we were unable to measure any intensity decay. Therefore, we concluded that any emission from the PIL-Cl was negligible. Figure 5 shows examples of the

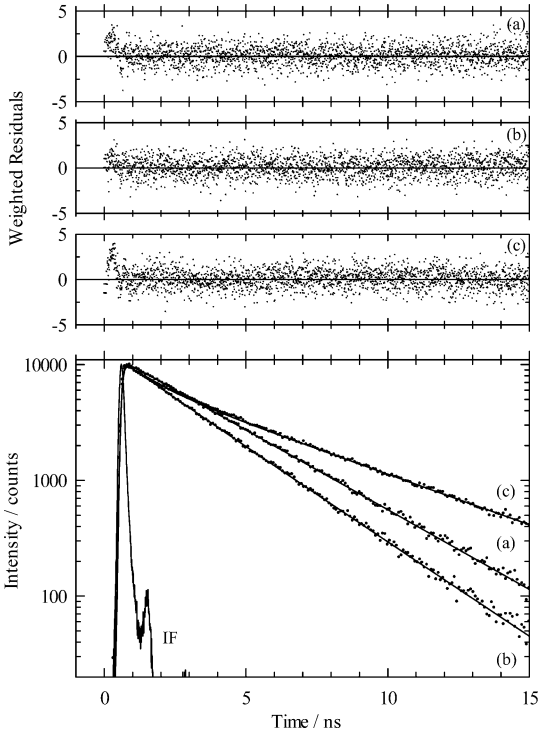

Figure 5. Examples of magic angle fluorescence intensity decays for C153 in PIL-Cl/MeOH at 295 K. The bottom panel shows decay data (points) and fits to these data (lines) for (a) x_{IL} = 0.002, (b) x_{IL} = 0.025, and (c) x_{IL} = 1. The line labeled "IF" is the instrument response function. The top panels show the weighted residuals at each of the mole fractions: (a) x_{IL} = 0.002 using two time constants in the decay model, (b) x_{IL} = 0.025 using three time constants in the decay model, and (c) x_{IL} = 1 using three time constants in the decay model.

emission intensity decay and fits to those data at x_{IL} = 0.002 (curve a), 0.025 (curve b), and 1 (curve c). Panels a, b, and c are the residuals of the fits at each of these mole fractions. The intensity decays are nonexponential for all but the four lowest values of x_{IL}, which required at least two time constants and typically three to achieve an acceptable fit (χ_r^2 < 1.2). A threshold of 10% improvement in χ_r^2 was used to determine whether additional time constants should be included when modeling the intensity decay data. Table 1 summarizes the exponential fit parameters to the intensity decay data. The average lifetime is computed using

$$\langle\tau\rangle = \frac{\sum_i a_i\tau_i^2}{\sum_i a_i\tau_i} \quad (1)$$

where a_i is the normalized unweighted pre-exponential values that were calculated directly from the DAS-6 fitting parameters and τ_i is the recovered lifetime. Given the time resolution of these experiments, the lifetime in neat MeOH is adequately described by a single time constant of 3.91 ns, which is in good agreement with previous measurements.[81] However, we note here that with much higher time resolution C153 in MeOH required four time constants to adequately model the entire intensity decay, and the longest time constant reported was 3.90 ns.[82] Our ~4 ns time constant is lower than the typical 6 ns lifetime for C153,[47] indicating that the nonradiative relaxation pathways are significantly enhanced. In contrast, the lifetime in neat PIL-Cl is best fit by a multiexponential decay model using three time constants and an average lifetime of 4.61 ns. The intensity decay in neat ILs (to our knowledge) is characteristically nonexponential,[47,51,52,79,83] requiring up to five exponentials to fit the intensity decay data,[83] because of the inherently complex nature of the medium and thus the nature of probe solvation. Kim and co-workers identified anion translation with sub-picosecond dynamics and anion and cation diffusion with slow solvent dynamics,[18] and there are certainly other contributions to solute−solvent interactions that will influence the C153 intensity decay.[51] However, since our ultimate goal is to use the intensity decay data to obtain time-dependent emission spectra (see section III.E), we ascribe no particular relevance to the exact values of the time constants, as they are used simply to parametrize the intensity decay. Nonetheless, it is interesting to note two points here: (1) the value 5.18 ns is consistent with what was measured previously in an independent set of experiments;[52,53] (2) the longest time constants in the multiexponential fits essentially mimic those of the S_1 lifetime.[52] It is useful to visualize the dependence of $\langle\tau\rangle$ as a function of x_{IL}, and we plot that data in Figure 6. In addition to the lifetime data, we also include the lifetime-weighted fractional contributions to the intensity decay to give a better sense of the relative importance of each component. The fractions are calculated according to eq 2

$$f_i = \frac{a_i\tau_i}{\sum_i a_i\tau_i} \quad (2)$$

where a_i and τ_i are defined as in eq 1. Small additions of PIL-Cl to neat MeOH decrease the average lifetime rapidly down to a minimum of 2.57 ns at x_{IL} = 0.025. Although the steady-state intensity change was attributed to dilution, the lifetime data have no such explicit dependence on C153 concentration. These data demonstrate that the radiative rate of C153 is very sensitive to the PIL-Cl presence and that solute−solvent interactions are indeed changing, even at very low x_{IL}. The complexity of the system is increasing with added PIL-Cl, which is clearly indicated by the number of time constants needed to model the intensity decay. For example, two time constants are required to describe the intensity decay beginning at x_{IL} = 0.005 (▲ in Figure 6; see also Table 1), even though the contribution from the faster time constant (~700−800 ps) is only between 1 and 4%. The shape and magnitude of the lifetime changes at small x_{IL} roughly mirror the steady-state intensity trend with an observed minimum value at x_{IL} ~0.03 followed by a systematic increase of radiative decay up to x_{IL} = 1. Another feature that is evident in Figure 6 is the use of three time constants (●) in the intensity decay fits, coincident with passing through the minimum in average lifetime. For x_{IL} > 0.03, the fastest time constant (τ_1, Table 1, ~200−300 ps) remains present and consistent with a contribution of only a few percent. The main variation in the fractional contribution is associated with the two longer decay times, and the dominant contribution (≥80%, open symbols, Figure 6a) is also the longest time constant at all x_{IL}. Thus, the shape of the average

dx.doi.org/10.1021/jp5092784 | J. Phys. Chem. B 2014, 118, 12979−12992

Table 1. Results of Intensity Decay Fits at 295 K Using Multi-Exponential Models

x_{IL}	a_1	a_2	a_3	τ_1 (ns)	τ_2 (ns)	τ_3 (ns)	χ_r^2	$\langle\tau\rangle^a$ (ns)
0			1.00			3.91	1.08	3.91
0.0002			1.00			3.81	1.12	3.81
0.0009			1.00			3.48	1.13	3.48
0.002			1.00			3.14	1.10	3.14
0.005		0.05	0.95		0.70	2.81	1.10	2.79
0.007		0.07	0.93		0.85	2.69	1.09	2.65
0.012		0.08	0.92		0.69	2.64	1.04	2.59
0.024	0.12	0.08	0.80	0.20	1.30	2.66	1.07	2.57
0.036	0.19	0.10	0.71	0.17	1.38	2.95	1.03	2.81
0.046	0.19	0.08	0.73	0.22	1.33	3.04	1.11	2.91
0.064[b]	0.28	0.10	0.63	0.22	1.45	3.35	1.07	3.15
0.068[c]	0.29	0.10	0.61	0.21	1.23	3.61	1.03	3.40
0.081[c]	0.29	0.10	0.61	0.25	1.34	3.83	1.06	3.59
0.088[b]	0.27	0.12	0.61	0.24	1.11	3.77	1.08	3.54
0.094[c]	0.30	0.14	0.56	0.24	1.27	4.04	1.03	3.74
0.10[b]	0.27	0.14	0.59	0.31	1.35	4.17	1.08	3.86
0.11[c]	0.30	0.14	0.55	0.27	1.33	4.22	1.04	3.89
0.12	0.28	0.17	0.55	0.28	1.27	4.34	1.06	3.97
0.15	0.24	0.19	0.57	0.30	1.33	4.54	1.04	4.15
0.17	0.27	0.24	0.49	0.29	1.40	4.68	1.13	4.15
0.20	0.27	0.27	0.46	0.37	1.61	4.79	1.07	4.14
0.26	0.23	0.28	0.49	0.35	1.88	4.92	1.09	4.27
0.35	0.24	0.28	0.49	0.36	1.88	4.92	1.07	4.26
0.46	0.25	0.26	0.49	0.30	2.05	4.97	1.07	4.30
0.70	0.24	0.24	0.52	0.32	2.11	5.01	1.10	4.43
1.00	0.24	0.24	0.53	0.31	2.14	5.18	1.08	4.61

[a]The average lifetime is calculated using eq 1. [b]Mole fractions of these solutions were prepared from additions to neat MeOH. [c]Mole fractions of these solutions were prepared from additions to neat ionic liquid.

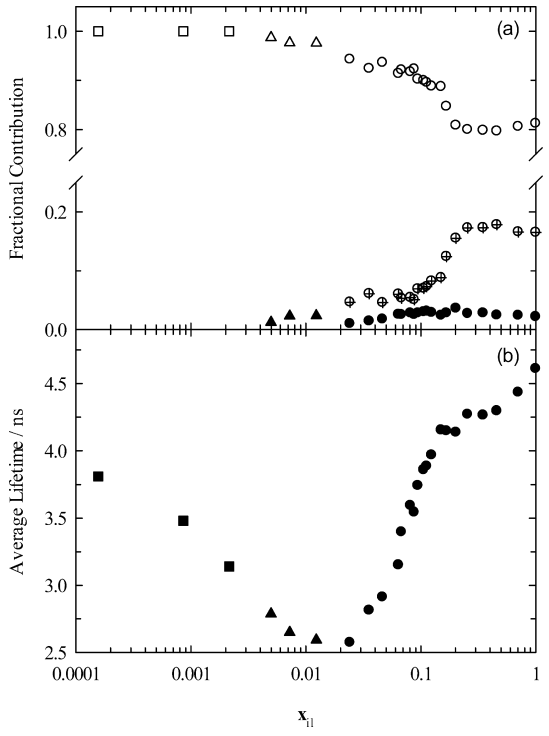

Figure 6. Fractional contributions and average lifetimes for C153 in PIL-Cl/MeOH solutions at 295 K. (a) Fractional contributions to the intensity decay for fits using one time constant (□), two time constants (△, ▲), and three time constants (○, ⊕, ●). (b) Average lifetimes calculated using eq 1 for best fit data with one time constant (■), two time constants (▲), and three time constants (●).

lifetime plot represents the change in the C153 S_1 lifetime. Whatever specific interactions are attributable to the two smaller time constants contribute at most 20% to the C153 decay kinetics.

D. Rotational Dynamics. Rotational dynamics of C153 were observed using fluorescence anisotropy decays measured at the peak of the emission spectrum at each solution mole fraction. Figure S4 (Supporting Information) shows representative polarized intensity decay data at x_{IL} = 0.086. The polarized intensity decays were fit using the sum of exponentials model

$$r(t) = r_0\left[\sum_{i=1}^{n} f_i \exp\left(\frac{-t}{\tau_{rot,i}}\right)\right] \quad (3)$$

where r_0 is the initial anisotropy, f_i is the normalized pre-exponential factor, and $\tau_{rot,i}$ is the rotation time. The values for r_0 were all contained within the range 0.34−0.39 except in dilute solution, as noted in Table 2. As a general trend, we note that as the PIL-Cl solution was diluted with MeOH r_0 systematically decreased, indicating that the limited time resolution of our measurements results in missing some portion of the faster components of the decay, hence necessitating fixing the value of r_0. The C153 anisotropy time constants show that in IL-rich solutions the rotational dynamics are complex, requiring up to three time constants to model the data. The results of these fits are summarized in Table 2, and the average rotational correlation times $\langle\tau_{rot}\rangle$ are plotted in Figure 7 as a function of solution viscosity. Also shown in Figure 7 (dashed lines) are the predicted hydrodynamic stick

dx.doi.org/10.1021/jp5092784 | J. Phys. Chem. B 2014, 118, 12979−12992

Table 2. Results of Anisotropy Decay Fits at 295 K[a]

x_{IL}	η (mPa·s)	f_1	f_2	f_3	τ_1 (ns)	τ_2 (ns)	τ_3 (ns)	$\langle\tau\rangle^b$ (ns)
0	0.54	1.00[c]			0.030			0.030 ± 0.003
0.0002	0.55	1.00[c]			0.033			0.033 ± 0.003
0.002	0.60	1.00[c]			0.034			0.034 ± 0.004
0.005	0.68	1.00[c]			0.045			0.045 ± 0.005
0.007	0.73	1.00[c]			0.049			0.049 ± 0.005
0.012	0.88	1.00[c]			0.059			0.059 ± 0.005
0.024	1.3	0.53	0.47		0.065	0.21		0.13 ± 0.03
0.035	1.8	0.46	0.54		0.070	0.28		0.18 ± 0.03
0.046	2.3	0.64	0.36		0.13	0.43		0.24 ± 0.03
0.067	3.7	0.51	0.49		0.14	0.66		0.40 ± 0.02
0.086	5.5	0.52	0.48		0.21	0.96		0.57 ± 0.03
0.11	8.8	0.46	0.54		0.26	1.36		0.85 ± 0.04
0.15	17.9	0.38	0.62		0.26	2.06		1.4 ± 0.04
0.17	24.9	0.38	0.62		0.31	2.38		1.6 ± 0.06
0.21	44.9	0.28	0.55	0.17	0.39	2.58	6.5[d]	2.6 ± 0.4
0.26	84.5	0.21	0.43	0.35	0.43	2.42	9.4[d]	4.6 ± 0.3
0.36	220	0.19	0.45	0.36	0.56	4.11	18.8[d]	9 ± 2
0.51	508	0.20	0.29	0.51	0.56	3.36	28.3[d]	18 ± 1[e]
0.71	846	0.15	0.27	0.57	0.48	3.50	37.7[d]	28 ± 4[e]
1.00	1995	0.09	0.26	0.65	0.35	3.53	68.6[d]	57 ± 5[e]

[a]Viscosities used here were calculated from a parametrization of the measured viscosities. [b]The average rotation time is calculated using $\sum_i f_i\tau_i$. [c]Caution should be used when interpreting these data points because they are at the extreme limit of our time resolution. These fits required that r_0 was fixed at 0.375, the value observed in vitrified solution.[84] [d]Data were fit by fixing the background to zero. [e]The average time for these mole fractions was calculated from the average of three replicates.

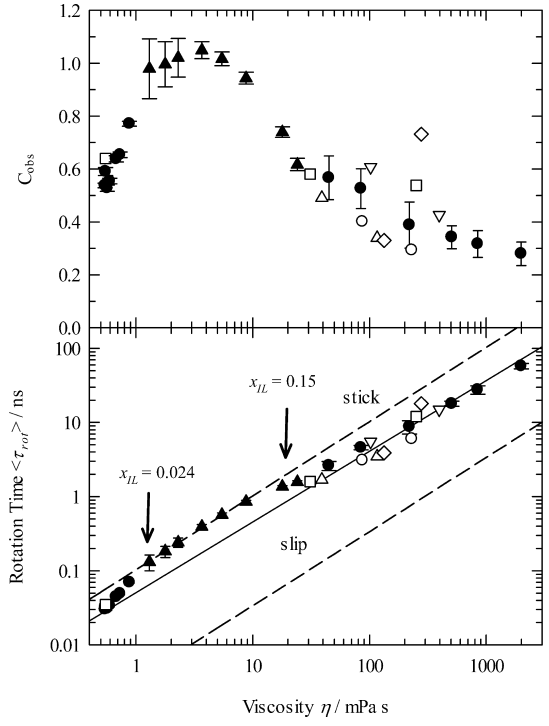

Figure 7. Average rotation times of C153 in PIL-Cl/MeOH at 295 K. Squares (■) represent fits using one rotation time, data sets shown by triangles (▲) used two rotation times, and circles (●) three rotation times. Open symbols are from prior work using this phosphonium cation with several anions: Br^- (△), Cl^- (▽), dicyanamide (◇), Tf_2N (○), and BF_4^- (□). The solid regression line is the fit to these data only.[52] The dashed lines in both plots represent the stick (upper line) and slip (lower line) hydrodynamic predictions. The solid line is the fit to the open symbols.

and slip limits for rotational diffusion computed using the relation

$$\tau_{hyd} = \frac{\eta V}{k_B T} fC \tag{4}$$

where V is C153 volume, f is a shape factor, and C is a coupling factor. Stick and slip predictions were calculated assuming that C153 is modeled as an ellipsoid with semiaxis dimensions of 2.0, 4.8, and 6.1 Å (V = 246 Å^3) and f = 1.71, with C = 1 and C = 0.24 for stick and slip limits, respectively.[84] To within experimental uncertainty, the observed rotation times all lie within these limiting predictions. The degree to which the observed rotation times correlate with hydrodynamic prediction can be quantified using rotational coupling factors, C_{obs},

$$C_{obs} = \frac{k_B T}{\eta V f} = \frac{\langle\tau_{rot}\rangle}{\tau_{stick}} \tag{5}$$

which are plotted in the upper panel of Figure 7. Also included in each panel are open symbols that show values of rotation times and coupling factors from previous work. The lone open square shown at 0.5 mPa·s is data for C153/MeOH measured at 22 °C using femtosecond up-conversion with 120 fs instrument response.[84] It is interesting to note that our rotation times at the lowest four mole fraction values (x_{IL} = 0.0002−0.005) yield the same value to within experimental uncertainties as C153 in neat MeOH measured by up-conversion. However, fitting these data required that we fix the initial anisotropy (r_0) to 0.375[84] in order to recover sensible rotation times, so we are very cautious not to overinterpret these points, since they lie at the extreme edge of our experimental time resolution.

At x_{IL} ~0.01 (η ~0.8 mPa·s), the C153 rotation times begin to show a marked difference from neat MeOH solution, and by x_{IL} = 0.024, the observed C153 rotations follow the stick limit hydrodynamic prediction. This behavior is readily apparent in

dx.doi.org/10.1021/jp5092784 | J. Phys. Chem. B 2014, 118, 12979−12992

the C_{obs} plot. Further, the trend in rotation times as it relates to solution mole fraction is consistent with other measurements presented here, most notably the maximum in solution conductivity, in that significant changes in solution organization occur up to x_{IL} = 0.024. The rotation data show clear evidence that PIL-Cl in solution becomes much more organized, since the rotational friction of C153 deviates substantially from neat MeOH (open square at 0.5 mPa·s). Evidently, the C153 microenvironment in the presence of PIL-Cl/MeOH between x_{IL} = 0.024 and 0.15 is such that the ion association with C153 and/or MeOH produces enough viscous drag that stick hydrodynamic theory is a good predictor of rotational diffusion. At x_{IL} ~0.15, the rotation times approach values that are similar to prior observations and we include the comparison data (Figure 7, open symbols) of $[P_{14,6,6,6}^+]$ paired with several anions (Br^- (△), Cl^- (▽), dicyanamide (◇), Tf_2N (○), and BF_4^- (□)) at various temperatures along with the regression (solid line) to that data.[52] Our rotation times at x_{IL} > 0.15 also show reasonable agreement with that work even though the anion dependence has a considerable spread in τ_{rot}. Our four highest mole fractions fall on that regression to within our experimental precision, as do our lowest mole fraction values. It is also noteworthy that at similar viscosity the PIL-Cl/MeOH rotation times match the neat Cl^- at higher temperature (▽). At least for these few mole fractions, it appears that the average C153 rotational dynamics do not differentiate between fluidity derived from composition-based solutions and thermal effects. Lastly, C_{obs} for our data for x_{IL} > 0.15 falls in the range of ~0.3−0.6, with an average value of $0.4_3 \pm 0.1_3$ in very good agreement with values and averages based on the 21 ionic liquids presented in ref 47.

E. Solvation Dynamics. Wavelength-resolved intensity decays of C153 in ionic liquids are observed to be highly nonexponential.[52,76,83] In these measurements, we used a series of 15−18 wavelengths to time resolve the C153 emission spectrum at each mole fraction, over the complete range of mole fraction. As an example, intensity decays for 3 of 18 wavelengths that were used in the reconstruction of the time-dependent emission spectra at x_{IL} = 0.086 are shown in Figure 8. The lower panel shows the data (points) and the fit to the data (lines) at 440 nm, the bluest wavelength measured, an intermediate value of 500 nm, and at 610 nm on the red edge of emission. The upper, smaller panels show the residuals for each of the fits and clearly show no systematic bias in the fits. The data were fit to a sum-of-exponentials model using a global analysis approach, assuming that the number time constants that describe the intensity decay remain the same at all wavelengths and that only the relative contribution varies. Using this approach, we find that at the lowest x_{IL} values only two time constants are needed to adequately model the data; however, as the amount of PIL-Cl increases, we require up to five exponential terms to fit the data. Similarly, Castner and co-workers[83] have reported that up to five exponentials were used to fit ammonium and pyrrolidinium IL decays.

From the intensity decay data, time-dependent emission spectra were reconstructed using the standard approach.[85] We calculated time-dependent emission spectra using 50 logarithmically spaced times across a window of 10 ps to 20 ns. Figure 9 presents some examples of the normalized spectra for several time increments at x_{IL} = 0.086. The symbols are the calculated values for the emission spectra, and the solid lines are those data sets fitted to a log-normal line shape. Also shown as dashed lines are the estimated time-zero[86] (t = 0) and measured

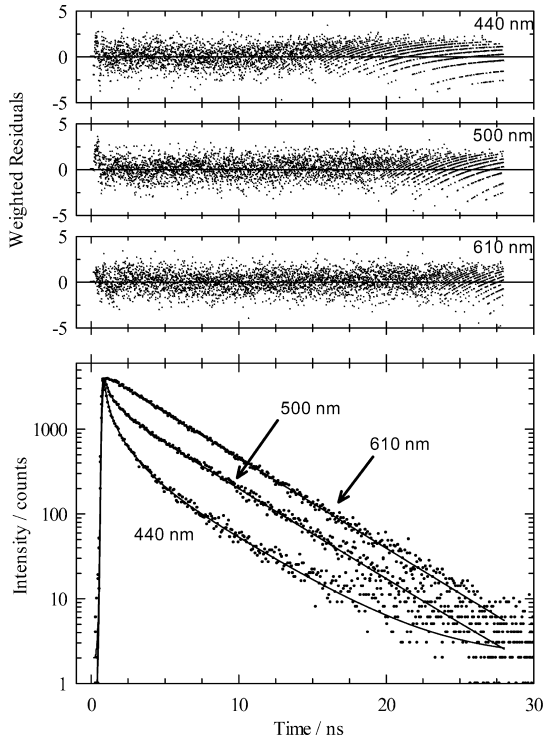

Figure 8. Representative emission wavelength dependent intensity decays, fits, and residuals of C153/PIL-Cl/MeOH; shown here are data for three of the 18 wavelength-dependent data sets at x_{IL} = 0.086 and 295 K. The bottom panel shows decay data at 440 nm, the bluest wavelength measured; 500 nm, an intermediate wavelength; and 610 nm, at the red edge of emission for this x_{IL}. The TCSPC data are shown as points and fits to a four-exponential global analysis model are shown as lines. The three upper panels show the weighted residuals at each of the emission wavelengths.

steady-state emission spectra (ss). The complete details of the time-zero calculation were reported by Fee and Maroncelli.[86] Briefly, the time-zero spectrum shown in Figure 9 was estimated by measuring the absorption and emission of C153 in a nonpolar reference solvent (in this work, 2-methylbutane) and using the line shapes from these spectra to calculate an expected shift and width that gives the closest match to the absorption spectrum of C153 in a given PIL-Cl/MeOH solution. Finally, the time-zero spectrum was calculated for the excitation frequency used in these experiments. The gap between the t = 0 spectrum and the 50 ps curve shows that in these measurements we are missing roughly 50% of the solvation because of limited time resolution (~40 ps after deconvolution of the instrument response function from the measured fluorescence intensity decay). The peak frequencies of the time-dependent spectra, $\nu(t)$, are plotted as logarithmically spaced points in the lower panel of Figure 9 at x_{IL} = 0.012, 0.024, 0.086, and 1; the lines show fits to those data using a stretched-exponential function

$$\nu(t) = \nu_\infty + \Delta\nu \exp\left(\frac{-t}{\tau_{solv}}\right)^{\beta_{solv}} \quad (6)$$

where ν_∞ is the peak frequency of the fully relaxed spectrum (≈steady-state emission), $\Delta\nu$ is the dynamic Stokes shift, t is the time, and τ_{solv} is the solvation time. The exponent β_{solv} is a measure of departure from exponential response. We did attempt to fit the data to a multiexponential model, but there

dx.doi.org/10.1021/jp5092784 | J. Phys. Chem. B 2014, 118, 12979−12992

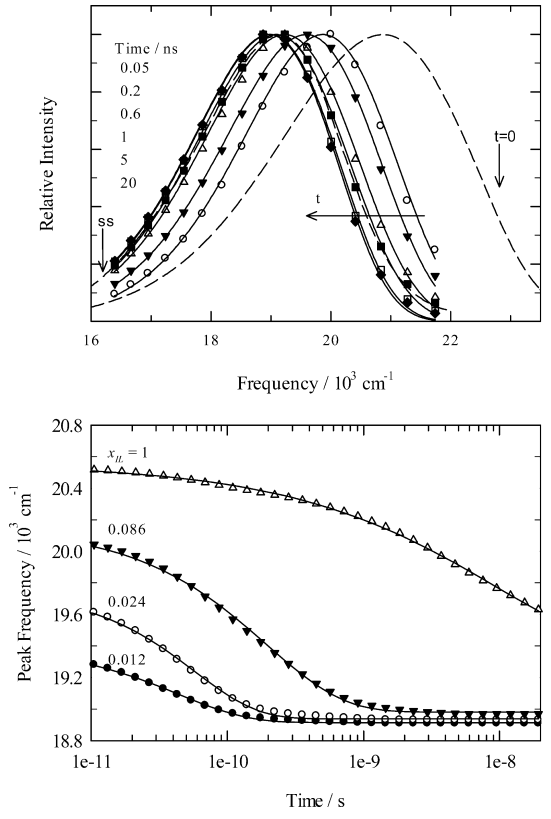

Figure 9. Upper panel: time-resolved emission spectra of C153 in PIL-Cl/MeOH at 295 K; x_{IL} = 0.086. The reconstructed data are shown as points at the times indicated, and the solid lines represent fits to a log-normal line shape function. The dashed curves are the steady-state (ss) and estimated time zero (t = 0) spectra. Lower panel: representative time dependent peak frequency data, $\nu(t)$, from log-normal fits of the time-resolved emission spectra. Data are shown as points, and the lines are the fits to the data using a stretched-exponential function.

was no significant improvement in the fits. Fitting results for ν_∞, $\Delta\nu$, τ_{solv}, and β_{solv} from eq 6 are summarized in Table 3. The estimated uncertainty in our peak frequencies is at most ±180 cm^{-1} based on replicate analyses. Also included are the values for the fraction of spectral shift measured (f_{obs}); the estimated uncertainty in these data is at most ±0.1. In these measurements, we observe that the Stokes shift varies from about 500 to 1300 cm^{-1} across the range of x_{IL}. Although we are able to characterize the complete solvation response, insofar as f_{obs} indicates, it is certain that even in the steady-state limit at 295 K the PIL-Cl solution has not completely relaxed. In neat PIL-Cl at 295 K, our ν_∞ value is 1000−1200 cm^{-1} higher than data at 331 K[53] and 343 K[52] where viscosities are roughly a factor of 10-fold lower. Also evident from these results is the inherent complexity of IL solutions as $x_{IL} \rightarrow 1$, which is clearly shown by the highly nonexponential solvation behavior, indicated by the decreasing β_{solv} values. In dilute solution, we see that $\beta_{solv} \approx 1$ and decreases to ∼0.5 in PIL-Cl-rich solutions.

The viscosity dependence of the C153 solvation times (●) is plotted in Figure 10 along with phosphonium IL data from ref

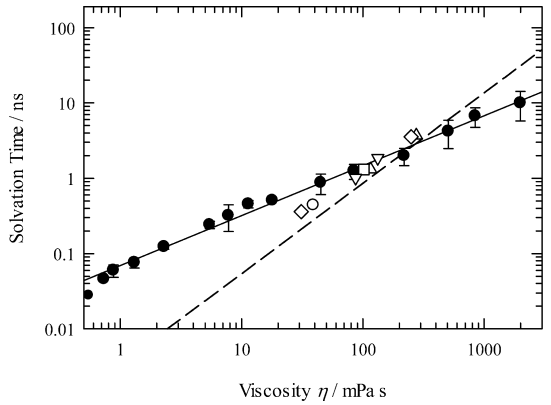

Figure 10. Viscosity dependence of the average solvation times of C153 in PIL-Cl/MeOH at 295 K. The solvation times are calculated from the average of three replicates that were fitted to a stretched-exponential model. The solid line is the fit to the MeOH data only, excluding the two lowest points: $\ln(\tau_{solv}/ns) = -1.16 + 0.66 \ln(\eta/mPa{\cdot}s)$, r^2 = 0.99. Open symbols are from prior work using this phosphonium cation with several anions: Br$^-$ (△), Cl$^-$ (▽), dicyanamide (◇), Tf$_2$N (○), and BF$_4^-$ (□).[52] The dashed line is the reported correlation, which includes conventional dipolar solvent data and ILs. See details in ref 52.

Table 3. Results of Stretched-Exponential Fits to Time-Dependent Peak Frequencies at 295 K

x_{IL}	η^a (mPa·s)	$\nu(\infty)$ (10^{-3} cm^{-1})	$\Delta\nu$ (10^{-3} cm^{-1})	τ_{solv} (ns)	β_{solv}	$f_{obs}{}^b$
0.0002[c]	0.55	18.85	0.66	0.029 ± 0.004	1.00	
0.007[c]	0.73	18.88	0.56	0.04 ± 0.01	1.02	
0.012	0.88	18.91	0.48	0.06 ± 0.01	0.88	0.41
0.024	1.3	18.94	0.81	0.07 ± 0.01	0.93	0.44
0.046	2.3	18.94	0.97	0.12 ± 0.01	0.89	0.49
0.086	5.5	18.98	1.17	0.24 ± 0.03	0.78	0.60
0.10	7.8	18.93	1.24	0.3 ± 0.1	0.71	0.64
0.12	11.4	18.99	1.12	0.5 ± 0.1	0.67	0.58
0.13	17.9	19.11	1.32	0.5 ± 0.1	0.63	0.73
0.20	44.9	19.19	1.33	0.9 ± 0.3	0.65	0.78
0.26	84.5	19.04	1.16	1.2 ± 0.3	0.60	0.64
0.35	220	19.21	0.93	2.0 ± 0.5	0.55	0.60
0.46	508	19.33	1.12	4 ± 2	0.55	0.82
0.71	846	19.47	1.10	7 ± 2	0.55	1.07
1.00	1995	19.46	1.08	10 ± 4	0.53	1.06

[a]Viscosities used here were calculated from a parametrization of the measured viscosities. [b]$f_{obs} = [(\nu(t) - \nu(\infty)]/[\nu(0) - \nu(\infty)]$ is the fraction of spectral shift measured. The estimated uncertainty is ±0.1. [c]Caution should be used when interpreting these solvation times because they are at the extreme limit of our time resolution (∼40 ps). They are included largely for relative comparison and should not be overinterpreted.

dx.doi.org/10.1021/jp5092784 | J. Phys. Chem. B 2014, 118, 12979−12992

52 (open symbols). The solid line is the regression to the MeOH data only. We note that, because of limited time resolution in these TCSPC measurements, the τ_{solv} times at the two lowest x_{IL} values (lowest viscosity points) lie at the extreme edge of measurement and therefore should be interpreted with caution. They are included here as mainly a qualitative comparison to the remaining data and were not used in calculating the regression line. In dilute PIL-Cl, solvent relaxation is about 2 orders of magnitude faster compared to neat PIL-Cl shown here, but it is significantly slower than that in conventional dipolar solvents. The dashed line is the fit to C153 solvation times in a broad range of solvents including various aprotic, protic, alcohol, and IL solvents taken from ref 47. The open symbols are solvation times for phosphonium ILs from ref 52. Two features are of interest here. First, the C153/PIL-Cl/MeOH data follow a linear correlation to solution viscosity (solid line) with the exception of the two lowest points, which are C153 in very dilute PIL-Cl solution. Second, these data show a distinctly different correlation compared to the composite data (-----). The linear dependence of solvation (and rotation) times on bulk solvent viscosity has been consistently reported in the IL literature, and in this regard, our data are not unique. However, in PIL-Cl/MeOH solution, the solvation times are generally slower except in more viscous solutions, greater than ~500 mPa·s. It is also interesting to note that although the correlations are different the PIL-Cl solvation times at higher temperature ($\bigtriangledown$, Figure 10) are the same, to within our experimental uncertainty. Moreover, the remaining anion solvation times are also very similar to the PIL-Cl/MeOH data.

F. Discussion. Over the past several years, a large number of experiments and simulations, using predominantly imidazolium ILs, have depicted the solvent structure in IL solutions in various states of aggregation based on strong ion pair interactions in both neat and cosolvent modified IL systems.[23,24,26−29,33,63,66,68,69,87−90] Ion pairing in neat and cosolvent modified ILs has been a topic of intense study using both experimental[27−29,66,70,71,91] and computational[23,24,33,63,87,89,92] approaches. Reports have suggested that in neat ILs the solvent structure is observed to be microheterogeneous[93] or extended aggregation[28,63,69,88,89,94] particularly when the cation possesses longer alkyl chains,[27,50,89,90,95] as is the case with the PIL-Cl. As PIL-Cl is added to MeOH up to x_{IL} ~0.1, the observed change in each of the experimental parameters is suggestive of increasing solution complexity, e.g., IL aggregation, as suggested in many reports. Various inter- and intramolecular interactions among the ions and MeOH contribute to the overall solution organization. For example, $[C_{14,6,6,6}^{+}]$ cation tail interactions drive ion association through hydrophobic interactions. As x_{IL} increases, changes in PIL-Cl aggregation and relative solution mass combine to increase the solution viscosity. The combined effect is increased viscous drag on C153. The combination of solution mass increase from greater amounts of PIL-Cl in solution (the mass ratio PIL-Cl/MeOH is ~16-fold) and ion aggregation results in a bulk solution viscosity increase, and with these changes, the viscous drag on C153 increases. Although we cannot quantify the individual contributions, the effect is clearly evident from the measured viscosity changes and thus the C153 rotational dynamics. Further, rotation times clearly demonstrate that with added PIL-Cl the solution is organizing such that there is enhanced rotational friction experienced by C153. Although solution organization is increasing in complexity, a simple hydrodynamic model (e.g., bulk viscosity change) seems to reasonably account for the overall decrease in C153 mobility. It is interesting to note that the rotation times steadily increase toward the stick hydrodynamic limit with added PIL-Cl, although the reason for this increase is not completely clear using our data alone. Given the nature of the cation, one reasonable hypothesis is that the hydrophobic interactions between alkyl chains create a local structure with enough viscous drag that it ultimately reaches the hydrodynamic limit for rotational motion. We note here that a maximum in the conductivity data is observed at $x_{IL} \sim 0.025$. Evidently this solution composition represents the balance point between the competing effects of increasing ion concentration and decreasing ion mobility as bulk PIL-Cl solution is approached. Steady-state and lifetime data also indicate that $x_{IL} \sim 0.025$ is a point of significant change in solution behavior. The notion of spatial heterogeneity has been a common theme[50,93,96,97] predominantly focused on imidazolium ILs. Simulations have suggested the formation of domain-like structures, particularly with ionic liquids that possess long alkyl chains,[89,93,97] and our PIL-Cl data add to the growing body of evidence to support this general behavior.

We hypothesize that the local organization of ions is responsible, and since Cl^- is a small, hard, hydrophilic ion, it is reasonable to assume that hydrogen bonding to MeOH should encourage localization around the PIL-Cl ions. However, it is also instructive to consider the relative amounts of MeOH and PIL-Cl as a function of x_{IL}. We calculate that from $x_{IL} = 0$ to 0.025 the mol ratio of MeOH to PIL-Cl decreases by ~200-fold and beyond $x_{IL} = 0.025$ PIL-Cl is clearly the dominant component in solution. The steady-state emission maximum shows that up to $x_{IL} = 0.1$ the average C153 environment is still that of "MeOH". Thus, if formation of a nano- or microheterogenous structure is a good description for $x_{IL} = 0-0.1$ and C153 localizes near the ions, then the combination of increased local ion concentration[80] and dipolar interactions through ion−dipole and dipole−dipole coupling together are responsible for quenching the C153 fluorescence. This accounts for the additional diminution of intensity beyond simple dilution effects and provides at least a working hypothesis for the decrease in average lifetime. In addition, the collection of all of these effects could also help explain why the solvation times are significantly longer in the PIL-Cl/MeOH solutions compared to what has been observed in other IL work.[47]

As of yet, we have not addressed the steady-state intensity and average lifetime *increase* for $x_{IL} > 0.25$, especially between $0.025 < x_{IL} < 0.1$. Why should emission intensity and average lifetime increase as volume increases if only probe dilution were responsible for these changes? With less MeOH present, there is less hydrogen bonding with Cl^- ions and therefore less dipolar forces on the whole. Thus, while ion−dipole forces are still present, the data show that the C153 is on the whole increasingly more hydrophobic, which is consistent with a blue shift and longer average lifetime. Given that the average rotation time moves away from the stick limit at $x_{IL} \sim 0.15$, C153 must be experiencing some amount of decoupling from its local environment. Thus, on average, with less MeOH near C153, the dipolar contributions lessen, Cl^- hydrogen bonding decreases, and the hydrophobic and ion−dipole electrostatics increasingly govern the C153 emission. Solvation by PIL-Cl with lessened dipolar coupling shifts the emission maximum to higher energy and increases the average excited-state lifetime

because there are fewer nonradiative decay modes accessible to C153. Further evidence to support this hypothesis is apparent from the simulations. Maginn and co-workers[63] used molecular dynamics simulations to calculate the potential mean force (PMF) in $[C_n mim^+][Cl^-]$ and $[C_n mim^+][Tf_2N^-]$ ILs and showed that small, hard ions such as Cl^- paired with short chain IL cations are more weakly associated than longer chained IL cations paired with softer anions.

We now consider the IL-rich data. As previously mentioned, cation/anion identity impacts the strength of interactions and thus the relative rigidity in the aggregation network. The PIL-Cl ion pair network is in a state of extended aggregation, as confirmed by high viscosity (>1500 mPa·s) and low conductivity (~10 μS/cm), as observed in other neat ILs.[77,78,98−100] In bulk PIL-Cl, the longest time constant (5.18 ns) is still significantly less than the 6−7 ns decay time observed in conventional organic liquids.[52] In PIL-Cl and other similar PILs, Kashyap and Biswas have used a semimolecular theory based on first-principles and estimated that ion−dipole interactions account for ~75% of the C153 solvation dynamics and the remainder is from dipolar contributions.[55] It is interesting to note that our PIL-Cl lifetime data (x_{IL} = 1) yield results that qualitatively agree with this assessment. The calculated fractional contribution (see Figure 6) of the 5.18 ns time constant is about 80%, and the remaining 20% contribution to the decay is associated with relaxation that is on the order of 1 ns or less.

In the presence of MeOH cosolvent, our data collectively show that there is penetration of MeOH into the aggregated structure and the MeOH "loosens" the ionic liquid solution structure. In the range 0.1 < x_{IL} < 1, the steady-state emission (Figure 4) consistently shifts toward lower energy and the average lifetime (Figure 6) decreases, indicating dipolar coupling between C153 and MeOH strengthens. Viscosity data (Figure 1) clearly show that added MeOH disrupts the aggregated network, as evidenced by an increase in solution fluidity (η^{-1}). Buchner and co-workers[69] observed a substantial deviation from the neat IL response in $[bmim^+][BF_4^-]$/dichloromethane (DCM), with a maximum in static permittivity at x_{IL} ~ 0.08. On PIL-Cl dilution with MeOH, the trend in our lifetime data is similar to what Buchner reports. Their subsequent analysis reasoned that in a DCM-rich solution contact ion pairs are the dominant form of IL. The PIL-Cl/MeOH data also give a similar picture. With sufficient amounts of MeOH present, the ion pair network is disrupted and at low enough x_{IL} the solution behavior is consistent with conventional electrolyte solutions.

IV. SUMMARY AND CONCLUSIONS

Combining all the data in the $[P_{14,6,6,6}^+][Cl^-]$ /MeOH solvent system, we observe the following solution features. First, at very low mole fraction, x_{IL} < 0.001, the lifetime is well described by a single exponential decay, the solution viscosity is that of MeOH, solution conductivity is minimal, and the steady-state parameters indicate no variation in either C153 emission or fwhm. The rotation times agree well with what is expected in conventional organic solvents. From all these results, we conclude that the PIL-Cl solution structure is that of a typical electrolyte solution containing solvent-separated ions. However, with even the smallest addition of PIL-Cl (x_{IL} = 0.0002), the lifetime decrease indicates that C153 does sense the change in solution composition. Second, within a small mole fraction window at x_{IL} ~ 0.005, the intensity decay fits require two time constants, with greater than 98% of the contribution associated with the longer time constant. The rapidly increasing conductivity and marked increase in average rotation times support the idea that addition of PIL-Cl results in the onset of ion pairing and subsequent ion pair aggregation. Third, at x_{IL} ~ 0.025, C153 experiences an increasingly heterogeneous microenvironment where the average lifetime reaches a minimum value of 2.5 ns coincident with the requirement of three time constants needed to describe the intensity decay data. The fractional contributions show that the C153 decay kinetics that are associated with the ~1 ns time constant contribute much more significantly to the overall intensity decay. The C153 rotation time increases significantly, up to the stick hydrodynamic limit, although the corresponding solvation dynamics seem to strictly follow a linear viscosity correlation. Solution conductivity reaches a maximum value, and viscosity noticeably increases. These data all indicate that more substantial solution organization (e.g., aggregation) is occurring in solution. For x_{IL} > 0.03, ion pair aggregation steadily increases. C153's emissive characteristics (the increasing average lifetime, blue shifting emission maximum, increasing fwhm) along with changes in bulk solution properties (increasing viscosity and decreasing conductivity) together describe a system that shows greater hydrophobic character. We take this to indicate the formation of a network level system of organization. Lastly, for x_{IL} > 0.2, dramatic changes in the data have ceased with the exception of solution viscosity, and hence rotation and solvation dynamics that are directly proportional to solution viscosity, which continues to steadily increase until x_{IL} = 1. The dominant behavior of the system seems to be driven by PIL association, both ion−ion and hydrophobic tail interactions, and is manifested mostly through viscosity related observables.

■ ASSOCIATED CONTENT

Supporting Information

Density data as a function of x_{IL} are presented in Table S1. Figures S1 and S2 show viscosity and conductivity data plotted as a function of the molar concentration of PIL-Cl. Figure S3 presents a comparison of the relative intensity of the PIL-Cl emission blank and emission of C153 in PIL-Cl in the absence of MeOH. Figure S3 shows the relative intensity differences between the PIL-Cl blank and C153 in PIL-Cl. Figure S4 shows a set of polarized (parallel and perpendicular) emission intensity decays. This material is available free of charge via the Internet at http://pubs.acs.org.

■ AUTHOR INFORMATION

Corresponding Author

*E-mail: mheitz@brockport.edu. Phone: 585-395-5586.

Present Address

†Department of Chemistry, University of Rochester, Rochester, NY 14627.

Notes

The authors declare no competing financial interest.

■ ACKNOWLEDGMENTS

M.P.H. thanks Mark Maroncelli and Markus Hoffmann for many helpful discussions. The authors gratefully acknowledge support from the NSF-MRI program, grant award number CHE-0619320, and for support through the scholarly incentive grant program at The College at Brockport, SUNY.

REFERENCES

(1) Yue, C.; Fang, D.; Liu, L.; Yi, T.-F. Synthesis and Application of Task-Specific Ionic Liquids Used as Catalysts and/or Solvents in Organic Unit Reactions. *J. Mol. Liq.* **2011**, *163*, 99−121.

(2) *Ionic Liquids in Synthesis*; Wiley-VCH: Weinheim, Germany, 2003.

(3) *Ionic Liquids, Industrial Applications for Green Chemistry*; American Chemical Society: Washington, DC, 2002.

(4) Wilkes, J. S. A Short History of Ionic Liquids-from Molten Salts to Neoteric Solvents. *Green Chem.* **2002**, *4*, 73−80.

(5) Paul, S.; Panda, A. K. Physicochemical Investigations on the Aqueous Solution of an Ionic Liquid, 1-Butyl-3-Methylimidazolium Methanesulfonate, [Bmim][Ms], in a Concentrated and Dilute Regime. *Colloids Surf., A* **2012**, *404*, 1−11.

(6) Weingärtner, H.; Knocks, A.; Schrader, W.; Kaatze, U. Dielectric Spectroscopy of the Room Temperature Molten Salt Ethylammonium Nitrate. *J. Phys. Chem. A* **2001**, *105*, 8646−8650.

(7) Lee, J.-M.; Prausnitz, J. M. Polarity and Hydrogen-Bond-Donor Strength for Some Ionic Liquids: Effect of Alkyl Chain Length on the Pyrrolidinium Cation. *Chem. Phys. Lett.* **2010**, *492*, 55−59.

(8) Liu, X.; Afzal, W.; Yu, G.; He, M.; Prausnitz, J. M. High Solubilities of Small Hydrocarbons in Trihexyl Tetradecylphosphonium Bis(2,4,4-Trimethylpentyl) Phosphinate. *J. Phys. Chem. B* **2013**, *117*, 10534−10539.

(9) Lawler, C.; Fayer, M. D. The Influence of Lithium Cations on Dynamics and Structure of Room Temperature Ionic Liquids. *J. Phys. Chem. B* **2013**, *117*, 9768−9774.

(10) Fletcher, K. A.; Pandey, S. Effect of Water on the Solvatochromic Probe Behavior within Room-Temperature Ionic Liquid 1-Butyl-3-Methylimidazolium Hexafluorophosphate. *Appl. Spectrosc.* **2002**, *56*, 266−271.

(11) Swatloski, R. P.; Visser, A. E.; Reichert, W. M.; Broker, G. A.; Farina, L. M.; Holbrey, J. D.; Rogers, R. D. On the Solubilization of Water with Ethanol in Hydrophobic Hexafluorophosphate Ionic Liquids. *Green Chem.* **2002**, *4*, 81−87.

(12) Ghalami-Choobar, B.; Shekofteh-Gohari, M. Determination and Modeling of Activity Coefficients of the Ionic Liquid 1-Ethyl-3-Methylimidazolium Chloride in the (Water + Formamide) Mixed Solvent System at 298.2 K. *J. Mol. Liq.* **2013**, *180*, 154−159.

(13) Batista, M. L. S.; Neves, C. M. S. S.; Carvalho, P. J.; Gani, R.; Coutinho, J. A. P. Chameleonic Behavior of Ionic Liquids and Its Impact on the Estimation of Solubility Parameters. *J. Phys. Chem. B* **2011**, *115*, 12879−12888.

(14) Yoo, B.; Afzal, W.; Prausnitz, J. M. Solubility Parameters for Nine Ionic Liquids. *Ind. Eng. Chem. Res.* **2012**, *51*, 9913−9917.

(15) Mandal, P. K.; Paul, A.; Samanta, A. Excitation Wavelength Dependent Fluorescence Behavior of the Room Temperature Ionic Liquids and Dissolved Dipolar Solutes. *J. Photochem. Photobiol., A* **2006**, *182*, 113−120.

(16) Yeganegi, S.; Soltanabadi, A.; Farmanzadeh, D. Molecular Dynamic Simulation of Dicationic Ionic Liquids: Effects of Anions and Alkyl Chain Length on Liquid Structure and Diffusion. *J. Phys. Chem. B* **2012**, *116*, 11517−11526.

(17) Znamenskiy, V.; Kobrak, M. N. Molecular Dynamics Study of Polarity in Room-Temperature Ionic Liquids. *J. Phys. Chem. B* **2004**, *108*, 1072−1079.

(18) Shim, Y.; D, J.; Choi, M. Y.; Kim, H.-J. Solvation in Molecular Ionic Liquids. *J. Chem. Phys.* **2003**, *119*, 6411−6414.

(19) Hanke, C. G.; Atamas, N. A.; Lynden-Bell, R. M. Solvation of Small Molecules in Imidazolium Ionic Liquids: A Simulation Study. *Green Chem.* **2002**, *4*, 107−111.

(20) Cho, C.-W.; Preiss, U.; Jungnickel, C.; Stolte, S.; Arning, J.; Ranke, J.; Klamt, A.; Krossing, I.; Thöming, J. Ionic Liquids: Predictions of Physicochemical Properties with Experimental and/or Dft-Calculated Lfer Parameters to Understand Molecular Interactions in Solution. *J. Phys. Chem. B* **2011**, *115*, 6040−6050.

(21) Lü, R.; Qu, Z.; Yu, H.; Wang, F.; Wang, S. Comparative Study on Interactions between Ionic Liquids and Pyridine/Hexane. *Chem. Phys. Lett.* **2012**, *532*, 13−18.

(22) Xuan, X.; Guo, M.; Pei, Y.; Zheng, Y. Theoretical Study on Cation−Anion Interaction and Vibrational Spectra of 1-Allyl-3-Methylimidazolium-Based Ionic Liquids. *Spectrochim. Acta, Part A* **2011**, *78*, 1492−1499.

(23) Kobrak, M. N. Characterization of the Solvation Dynamics of an Ionic Liquid Via Molecular Dynamics Simulation. *J. Chem. Phys.* **2006**, *125*, 064502-1−064502-11.

(24) Kobrak, M. N. A Comparative Study of Solvation Dynamics in Room-Temperature Ionic Liquids. *J. Chem. Phys.* **2007**, *127*, 184507-1−184507-8.

(25) Matkowska, D.; Hofman, T. Volumetric Properties of the Ionic Liquids: [C6mim][Meso4], [C6mim][Etso4], [C4mim][Etso4] and Their Mixtures with Methanol or Ethanol. *J. Mol. Liq.* **2013**, *177*, 301−305.

(26) Tubbs, J. T.; Hoffmann, M. M. Ion-Pair Formation of the Ionic Liquid 1-Ethyl-3-Methylimidazolium Bis(Trifyl)Imide in Low Dielectric Media. *J. Solution Chem.* **2004**, *33*, 381−394.

(27) Scharf, N. T.; Stark, A.; Hoffmann, M. M. Ion Pairing and Dynamics of the Ionic Liquid 1-Hexyl-3-Methylimidazolium Bis-(Irifluoromethylsulfonyl)Amide ([C6mim][Ntf2]) in the Low Dielectric Solvent Chloroform. *J. Phys. Chem. B* **2012**, *116*, 11488−11497.

(28) Scharf, N. T.; Stark, A.; Hoffmann, M. M. Calorimetric Study on the Ion Pairing and Aggregation of 1-Ethyl-3-Methylimidazolium Bis(Trifluoromethylsulfonyl)Amide ([C2mim][Ntf2]) and Related Ionic Liquids in the Low-Dielectric Constant Solvent Chloroform. *J. Solution Chem.* **2013**, *42*, 2034−2056.

(29) Jiang, Y.; Nadolny, H.; Kashammer, S.; Weibels, S.; Schroer, W.; Weingartner, H. The Ion Speciation of Ionic Liquids in Molecular Solvents of Low and Medium Polarity. *Faraday Discuss.* **2012**, *154*, 391−407.

(30) Ding, Z.-D.; Chi, Z.; Gu, W.-X.; Gu, S.-M.; Wang, H.-J. Theoretical and Experimental Investigation of the Interactions between [Emim]Ac and Water Molecules. *J. Mol. Struct.* **2012**, *1015*, 147−155.

(31) Chen, Y.; Cao, Y.; Sun, X.; Mu, T. Hydrogen Bonding Interaction between Acetate-Based Ionic Liquid 1-Ethyl-3-Methylimidazolium Acetate and Common Solvents. *J. Mol. Liq.* **2014**, *190*, 151−158.

(32) Huddleston, J. G.; Visser, A. E.; Reichert, W. M.; Willauer, H. D.; Broker, G. A.; Rogers, R. D. Characterization and Comparison of Hydrophilic and Hydrophobic Room Temperature Ionic Liquids Incorporating the Imidazolium Cation. *Green Chem.* **2001**, *3*, 156−164.

(33) Annapureddy, H. V.; Dang, L. X. Pairing Mechanism among Ionic Liquid Ions in Aqueous Solutions: A Molecular Dynamics Study. *J. Phys. Chem. B* **2013**, *117*, 8555−8560.

(34) Sarkar, S.; Mandal, S.; Ghatak, C.; Rao, V. G.; Ghosh, S.; Sarkar, N. Photoinduced Electron Transfer in an Imidazolium Ionic Liquid and in Its Binary Mixtures with Water, Methanol, and 2-Propanol: Appearance of Marcus-Type of Inversion. *J. Phys. Chem. B* **2011**, *116*, 1335−1344.

(35) Sarkar, S.; Pramanik, R.; Ghatak, C.; Setua, P.; Sarkar, N. Probing the Interaction of 1-Ethyl-3-Methylimidazolium Ethyl Sulfate ([Emim][Etso4]) with Alcohols and Water by Solvent and Rotational Relaxation. *J. Phys. Chem. B* **2010**, *114*, 2779−2789.

(36) Pramanik, R.; Rao, V. G.; Sarkar, S.; Ghatak, C.; Setua, P.; Sarkar, N. To Probe the Interaction of Methanol and Acetonitrile with the Ionic Liquid N,N,N-Trimethyl-N-Propyl Ammonium Bis-(Trifluoromethanesulfonyl) Imide at Different Temperatures by Solvation Dynamics Study. *J. Phys. Chem. B* **2009**, *113*, 8626−8634.

(37) Chakrabarty, D.; Chakraborty, A.; Seth, D.; Sarkar, N. Effect of Water, Methanol, and Acetonitrile on Solvent Relaxation and Rotational Relaxation of Coumarin 153 in Neat 1-Hexyl-3-Methylimidazolium Hexafluorophosphate. *J. Phys. Chem. A* **2005**, *109*, 1764−1769.

(38) Das, S. K.; Sarkar, M. Steady-State and Time-Resolved Fluorescence Behavior of Coumarin-153 in a Hydrophobic Ionic Liquid and Ionic Liquid−Toluene Mixture. *J. Mol. Liq.* **2012**, *165*, 38−43.

(39) Wu, W.; Li, W.; Han, B.; Jiang, T.; Shen, D.; Zhang, Z.; Sun, D.; Wang, B. Effect of Organic Cosolvents on the Solubility of Ionic Liquids in Supercritical Co_2. *J. Chem. Eng. Data* **2004**, *49*, 1597−1601.
(40) Paul, A.; Samanta, A. Effect of Nonpolar Solvents on the Solute Rotation and Solvation Dynamics in an Imidazolium Ionic Liquid. *J. Phys. Chem. B* **2008**, *112*, 947−953.
(41) Baker, S. N.; Baker, G. A.; Kane, M. A.; Bright, F. V. The Cybotactic Region Surrounding Fluorescent Probes Dissolved in 1-Butyl-3-Methylimidazolium Hexafluorophosphate: Effects of Temperature and Added Carbon Dioxide. *J. Phys. Chem. B* **2001**, *105*, 9663−9668.
(42) Kumełan, J.; Tuma, D.; Maurer, G. Simultaneous Solubility of Carbon Dioxide and Hydrogen in the Ionic Liquid [Hmim][Tf2n]: Experimental Results and Correlation. *Fluid Phase Equilib.* **2011**, *311*, 9−16.
(43) Jang, S.; Cho, D.-W.; Im, T.; Kim, H. High-Pressure Phase Behavior of Co2 + 1-Butyl-3-Methylimidazolium Chloride System. *Fluid Phase Equilib.* **2010**, *299*, 216−221.
(44) Bates, E. D.; Mayton, R. D.; Ntai, I.; Davis, J. H., Jr. Co_2 Capture by a Task-Specific Ionic Liquid. *J. Am. Chem. Soc.* **2002**, *124*, 926−927.
(45) Baltus, R. E.; Culbertson, B. H.; Dai, S.; Luo, H.; DePaoli, D. W. Low-Pressure Solubility of Carbon Dioxide in Room-Temperature Ionic Liquids Measured with a Quartz Crystal Microbalance. *J. Phys. Chem. B* **2004**, *108*, 721−727.
(46) Chakrabarty, D.; Chakraborty, A.; Seth, D.; Hazra, P.; Sarkar, N. Dynamics of Solvation and Rotational Relaxation of Coumarin 153 in 1-Butyl-3-Methylimidazolium Hexafluorophosphate [Bmim][Pf6]-Water Mixtures. *Chem. Phys. Lett.* **2004**, *397*, 469−474.
(47) Jin, H.; Baker, G. A.; Arzhantsev, S.; Dong, J.; Maroncelli, M. Solvation and Rotational Dynamics of Coumarin 153 in Ionic Liquids: Comparisons to Conventional Solvents. *J. Phys. Chem. B* **2007**, *111*, 7291−7302.
(48) Das, K. S.; Sarkar, M. Solvation and Rotational Relaxation of Coumarin 153 in a New Hydrophobic Ionic Liquid: An Excitation Wavelength Dependence Study. *J. Lumin.* **2012**, *132*, 368−374.
(49) Das, S. K.; Sarkar, M. Solvation and Rotational Relaxation of Coumarin 153 and 4-Aminophthalimide in a New Hydrophobic Ionic Liquid: Role of N−H···F Interaction on Solvation Dynamics. *Chem. Phys. Lett.* **2011**, *515*, 23−28.
(50) Mukherjee, P.; Crank, J. A.; Sharma, P. S.; Wijeratne, A. B.; Adhikary, R.; Bose, S.; Armstrong, D. W.; Petrich, J. W. Dynamic Solvation in Phosphonium Ionic Liquids: Comparison of Bulk and Micellar Systems and Considerations for the Construction of the Solvation Correlation Function, C(T). *J. Phys. Chem. B* **2008**, *112*, 3390−3396.
(51) Samanta, A. Solvation Dynamics in Ionic Liquids: What We Have Learned from the Dynamic Fluorescence Stokes Shift Studies. *J. Phys. Chem. Lett.* **2010**, *1*, 1557−1562.
(52) Ito, N.; Arzhantsev, S.; Heitz, M.; Maroncelli, M. Solvation Dynamics and Rotation of Coumarin 153 in Alkylphosphonium Ionic Liquids. *J. Phys. Chem. B* **2004**, *108*, 5771−5777.
(53) Arzhantsev, S.; Ito, N.; Heitz, M.; Maroncelli, M. Solvation Dynamics of Coumarin 153 in Several Classes of Ionic Liquids: Cation Dependence of the Ultrafast Component. *Chem. Phys. Lett.* **2003**, *381*, 278−286.
(54) Chakraborty, A.; Seth, D.; Chakrabarty, D.; Setua, P.; Sarkar, N. Dynamics of Solvent and Rotational Relaxation of Coumarin 153 in Room-Temperature Ionic Liquid 1-Butyl-3-Methylimidazolium Hexafluorophosphate Confined in Brij-35 Micelles: A Picosecond Time-Resolved Fluorescence Spectroscopic Study. *J. Phys. Chem. A* **2005**, *109*, 11110−11116.
(55) Kashyap, H. K.; Biswas, R. Solvation Dynamics of Dipolar Probes in Dipolar Room Temperature Ionic Liquids: Separation of Ion−Dipole and Dipole−Dipole Interaction Contributions. *J. Phys. Chem. B* **2010**, *114*, 254−268.
(56) Daschakraborty, S.; Pal, T.; Biswas, R. Stokes Shift Dynamics of Ionic Liquids: Solute Probe Dependence, and Effects of Self-Motion, Dielectric Relaxation Frequency Window, and Collective Intermolecular Solvent Modes. *J. Chem. Phys.* **2014**, *139*, 164503.
(57) Daschakraborty, S.; Biswas, R. Composition Dependent Stokes Shift Dynamics in Binary Mixtures of 1-Butyl-3-Methylimidazolium Tetrafluoroborate with Water and Acetonitrile: Quantitative Comparison between Theory and Complete Measurements. *J. Phys. Chem. B* **2014**, *118*, 1327−1339.
(58) Kashyap, H. K.; Biswas, R. Stokes Shift Dynamics in Ionic Liquids: Temperature Dependence. *J. Phys. Chem. B* **2010**, *114*, 16811−16823.
(59) Daschakraborty, S.; Ranjit, B. Stokes Shift Dynamics in (Ionic Liquid + Polar Solvent) Binary Mixtures: Composition Dependence. *J. Phys. Chem. B* **2011**, *115*, 4011−4024.
(60) Kanzaki, R.; Mitsugi, T.; Fukuda, S.; Fujii, K.; Takeuchi, M.; Soejima, Y.; Takamuku, T.; Yamaguchi, T.; Umebayashi, Y.; Ishiguro, S.-i. Ion-Ion Interaction in Room Temperature Ionic Liquid 1-Ethyl-3-Methylimidazolium Tetrafluoroborate Studied by Large Angle X-Ray Scattering Experiment and Molecular Dynamics Simulations. *J. Mol. Liq.* **2009**, *147*, 77−82.
(61) Wang, Y.-g.; Chen, D.-x.; OuYang, X.-k. Viscosity Calculations for Ionic Liquid−Cosolvent Mixtures Based on Eyring's Absolute Rate Theory and Activity Coefficient Models. *J. Chem. Eng. Data* **2010**, *55*, 4878−4884.
(62) Bhargava, B. L.; Balasubramanian, S. Insights into the Structure and Dynamics of a Room-Temperature Ionic Liquid: Ab Initio Molecular Dynamics Simulation Studies of 1-N-Butyl-3-Methylimidazolium Hexafluorophosphate ([Bmim][Pf6]) and the [Bmim][Pf6]−Co2Mixture. *J. Phys. Chem. B* **2007**, *111*, 4477−4487.
(63) Yee, P.; Shah, J. K.; Maginn, E. J. State of Hydrophobic and Hydrophilic Ionic Liquids in Aqueous Solutions: Are the Ions Fully Dissociated? *J. Phys. Chem. B* **2013**, *117*, 12556−12566.
(64) Seth, D.; Sarkar, S.; Pramanik, R.; Ghatak, C.; Setua, P.; Sarkar, N. Photophysical Studies of a Hemicyanine Dye (Lds-698) in Dioxane−Water Mixture, in Different Alcohols, and in a Room Temperature Ionic Liquid. *J. Phys. Chem. B* **2009**, *113*, 6826−6833.
(65) Kumar, B.; Singh, T.; Rao, K. S.; Pal, A.; Kumar, A. Thermodynamic and Spectroscopic Studies on Binary Mixtures of Imidazolium Ionic Liquids in Ethylene Glycol. *J. Chem. Thermodyn.* **2012**, *44*, 121−127.
(66) Govinda, V.; Attri, P.; Venkatesu, P.; Venkateswarlu, P. Temperature Effect on the Molecular Interactions between Two Ammonium Ionic Liquids and Dimethylsulfoxide. *J. Mol. Liq.* **2011**, *164*, 218−225.
(67) Kimura, Y.; Kobayashi, A.; Demizu, M.; Terazima, M. Solvation Dynamics of Coumarin 153 in Mixtures of Carbon Dioxide and Room Temperature Ionic Liquids. *Chem. Phys. Lett.* **2011**, *513*, 53−58.
(68) Porter, A. R.; Liem, S. Y.; Popelier, P. L. A. Room Temperature Ionic Liquids Containing Low Water Concentrations-a Molecular Dynamics Study. *Phys. Chem. Chem. Phys.* **2008**, *10*, 4240−4248.
(69) Hunger, J.; Stoppa, A.; Buchner, R.; Hefter, G. From Ionic Liquid to Electrolyte Solution: Dynamics of 1-N-Butyl-3-N-Methylimidazolium Tetrafluoroborate/Dichloromethane Mixtures. *J. Phys. Chem. B* **2008**, *112*, 12913−12919.
(70) Schröder, C.; Rudas, T.; Neumayr, G.; Benkner, S.; Steinhauser, O. On the Collective Network of Ionic Liquid/Water Mixtures. I. Orientational Structure. *J. Chem. Phys.* **2007**, *127*, 234503-1−234503-9.
(71) Schröder, C.; Hunger, J.; Stoppa, A.; Buchner, R.; Steinhauser, O. On the Collective Network of Ionic Liquid/Water Mixtures. Ii. Decomposition and Interpretation of Dielectric Spectra. *J. Chem. Phys.* **2008**, *129*, 184501-1−184501-10.
(72) Fraser, K. J.; MacFarlane, D. R. Phosphonium-Based Ionic Liquids: An Overview. *Aust. J. Chem.* **2009**, *62*, 309−321.
(73) Shirota, H.; Fukazawa, H.; Fujisawa, T.; Wishart, J. F. Heavy Atom Substitution Effects in Non-Aromatic Ionic Liquids: Ultrafast Dynamics and Physical Properties. *J. Phys. Chem. B* **2010**, *114*, 9400−9412.
(74) Tsunashima, K.; Sugiya, M. Physical and Electrochemical Properties of Low-Viscosity Phosphonium Ionic Liquids as Potential Electrolytes. *Electrochem. Commun.* **2007**, *9*, 2353−2358.

(75) Bradaric, C. J.; Downard, A.; Kennedy, C.; Robertson, A. J.; Zhou, Y. Industrial Preparation of Phosphonium Ionic Liquids. *Green Chem.* **2003**, *5*, 143−152.
(76) Jin, H.; O'Hare, B.; Dong, J.; Arzhantsev, S.; Baker, G. A.; Wishart, J. F.; Benesi, A. J.; Maroncelli, M. Physical Properties of Ionic Liquids Consisting of the 1-Butyl-3-Methylimidazolium Cation with Various Anions and the Bis(Trifluoromethylsulfonyl)Imide Anion with Various Cations. *J. Phys. Chem. B* **2007**, *112*, 81−92.
(77) Zhu, A.; Wang, J.; Han, L.; Fan, M. Measurements and Correlation of Viscosities and Conductivities for the Mixtures of Imidazolium Ionic Liquids with Molecular Solutes. *Chem. Eng. J.* **2009**, *147*, 27−35.
(78) Stoppa, A.; Hunger, J.; Buchner, R. Conductivities of Binary Mixtures of Ionic Liquids with Polar Solvents†. *J. Chem. Eng. Data* **2009**, *54*, 472−479.
(79) Ingram, J. A.; Moog, R. S.; Ito, N.; Biswas, R.; Maroncelli, M. Solute Rotation and Solvation Dynamics in a Room-Temperature Ionic Liquid. *J. Phys. Chem. B* **2003**, *107*, 5926−5932.
(80) Pradhan, T.; Biswas, R. Electrolyte-Concentration and Ion-Size Dependence of Excited-State Intramolecular Charge-Transfer Reaction in (Alkylamino)Benzonitriles: Steady-State Spectroscopic Studies. *J. Phys. Chem. A* **2007**, *111*, 11514−11523.
(81) Bose, S.; Adhikary, R.; Mukherjee, P.; Song, X.; Petrich, J. W. Considerations for the Construction of the Solvation Correlation Function and Implications for the Interpretation of Dielectric Relaxation in Proteins. *J. Phys. Chem. B* **2009**, *113*, 11061−11068.
(82) Horng, M. L.; Gardecki, J. A.; Papazyan, A.; Maroncelli, M. Subpicosecond Measurements of Polar Solvation Dynamics: Coumarin 153 Revisited. *J. Phys. Chem.* **1995**, *99*, 17311−17337.
(83) Funston, A. M.; Fadeeva, T. A.; Wishart, J. F.; Castner, E. W. Fluorescence Probing of Temperature-Dependent Dynamics and Friction in Ionic Liquid Local Environments. *J. Phys. Chem. B* **2007**, *111*, 4963−4977.
(84) Horng, M.-L.; Gardecki, J. A.; Maroncelli, M. Rotational Dynamics of Coumarin 153: Time-Dependent Friction, Dielectric Friction, and Other Nonhydrodynamic Effects. *J. Phys. Chem. A* **1997**, *101*, 1030−1047.
(85) Maroncelli, M.; Fleming, G. R. Picosecond Solvation Dynamics of Coumarin 153: The Importance of Molecular Aspects of Solvation. *J. Chem. Phys.* **1987**, *86*, 6221−6239.
(86) Fee, R. S.; Maroncelli, M. Estimating the Time-Zero Spectrum in Time-Resolved Emission Measurements of Solvation Dynamics. *Chem. Phys.* **1994**, *183*, 235−247.
(87) Hu, X.; Lin, Q.; Gao, J.; Wu, Y.; Zhang, Z. Anion−Cation and Ion−Solvent Interaction of Some Typical Ionic Liquids in Solvents with Different Dielectric Constant. *Chem. Phys. Lett.* **2011**, *516*, 35−39.
(88) Dupont, J. On the Solid, Liquid and Solution Structural Organization of Imidazolium Ionic Liquids. *J. Braz. Chem. Soc.* **2004**, *15*, 341−350.
(89) Shimizu, K.; Bernardes, C. E. S.; Canongia Lopes, J. N. Structure and Aggregation in the 1-Alkyl-3-Methylimidazolium Bis-(Trifluoromethylsulfonyl)Imide Ionic Liquid Homologous Series. *J. Phys. Chem. B* **2014**, *118*, 567−576.
(90) Gangamallaiah, V.; Dutt, G. B. Effect of Alkyl Chain Length on the Rotational Diffusion of Nonpolar and Ionic Solutes in 1-Alkyl-3-Methylimidazolium-Bis(Trifluoromethylsulfonyl)Imides. *J. Phys. Chem. B* **2013**, *117*, 12261−12267.
(91) D'Angelo, P.; Zitolo, A.; Aquilanti, G.; Migliorati, V. Using a Combined Theoretical and Experimental Approach to Understand the Structure and Dynamics of Imidazolium-Based Ionic Liquids/Water Mixtures. 2. Exafs Spectroscopy. *J. Phys. Chem. B* **2013**, *117*, 12516−12524.
(92) Migliorati, V.; Zitolo, A.; D'Angelo, P. Using a Combined Theoretical and Experimental Approach to Understand the Structure and Dynamics of Imidazolium-Based Ionic Liquids/Water Mixtures. 1. Md Simulations. *J. Phys. Chem. B* **2013**, *117*, 12505−12515.
(93) Wang, Y.; Voth, G. A. Tail Aggregation and Domain Diffusion in Ionic Liquids. *J. Phys. Chem. B* **2006**, *110*, 18601−18608.
(94) Cha, S.; Shim, T.; Ouchi, Y.; Doseok, K. Characteristics of Visible Fluorescence from Ionic Liquids. *J. Phys. Chem. B* **2013**, *117*, 10818−10825.
(95) Hemmateenejad, B.; Safavi, A.; Dorostkar, S. Aggregation of Imidazolium Based Ionic Liquids in Binary Methanol−Water Solvents: A Linear Solvation Free Energy Relationship Study. *J. Mol. Liq.* **2011**, *160*, 35−39.
(96) Triolo, A.; Russina, O.; Bleif, H.-J.; Di Cola, E. Nanoscale Segregation in Room Temperature Ionic Liquids. *J. Phys. Chem. B* **2007**, *111*, 4641−4644.
(97) Canongia Lopes, J. N. A.; Pádua, A. A. H. Nanostructural Organization in Ionic Liquids. *J. Phys. Chem. B* **2006**, *110*, 3330−3335.
(98) Li, W.; Zhang, Z.; Zhang, J.; Han, B.; Wang, B.; Hou, M.; Xie, Y. Micropolarity and Aggregation Behavior in Ionic Liquid+Organic Solvent Solutions. *Fluid Phase Equilib.* **2006**, *248*, 211−216.
(99) Li, W.; Zhang, Z.; Han, B.; Hu, S.; Xie, Y.; Yang, G. Effect of Water and Organic Solvents on the Ionic Dissociation of Ionic Liquids. *J. Phys. Chem. B* **2007**, *111*, 6452−6456.
(100) Li, W.-J.; Han, B.-X.; Tao, R.-T.; Zhang, Z.-F.; Zhang, J.-L. Measurement and Correlation of the Ionic Conductivity of Ionic Liquid-Molecular Solvent Solutions. *Chin. J. Chem.* **2007**, *25*, 1349−1356.